Simplified Fourier Series Based Transistor Open-Circuit Fault Location Method in Voltage-Source Inverter Fed Induction Motor

FENG WU[1], (Member, IEEE), JIANWEN SUN[1], DEHONG ZHOU[2], (Member, IEEE), YANG LIU[3], (Senior Member, IEEE), TAO GENG[3], JIN ZHAO[3], (Senior Member, IEEE)

[1] School of Computer Science and Engineering, Nanyang Technological University, 50 Nanyang Ave, 639798, Singapore
[2] Electrical Computer Engineering Dept, University of Alberta, Canada
[3] Guangdong HUST Industrial Technology Research institute, Guangdong Province Key Laboratory of Digital Manufacturing Equipment, Key Laboratory of Image Processing and Intelligent Control of the Ministry of Education of China, School of Artificial Intelligence and Automation, Huazhong University of Science and Technology, Wuhan, 430074, China

Corresponding author: Jin Zhao (jinzhao617@163.com) and Dehong Zhou (dehong1@ualberta.ca).

This work was supported in part by the Guangdong Innovative and Entrepreneurial Research Team Program under Grant 2014ZT05G304 and in part by the National Natural Science Foundation of China under Grant 61573159, Grant 61273174.

ABSTRACT Transistors in three-phase voltage-source inverter often suffer from open-circuit failures due to the lifting of bonding wires caused by thermic cycling, resulting in performance degradation with ripple torque and current harmonics. Current-spectral-analysis based methods are widely applied to failure diagnosis; however, high calculation consumption and complex implementation limit their application in some real-time occasion. In this paper, a simplified Fourier series method is proposed by the product between reconstructed phase currents and reference signals. Meanwhile, a novel normalized method for DC and fundamental components of simplified Fourier series are proposed to locate twenty-one transistor open-circuit faults. Numerical results show that the proposed Fourier series method coincides with that of Fast Fourier Transform. Experimental results and the comparison with previous methods show high efficiency and merits of its application to transistor open-circuit fault location in the voltage-source inverter.

INDEX TERMS Voltage-source inverter, Real-time, Current spectral, Open-circuit, Fault location.

Nomenclature

VSI	Voltage-Source Inverter
IM	Induction Motor
FOC	Feild Oriented Control
CDR	Current Data Reconstruction
RLT	Rated Load Torque
FFT	Fast Fourier Transformation
ZCS	Zero-Crossing Sample
CL	Current Linklist
ω^*	rad/s, Reference Angle Speed
m	Representive of a, b, c
i_m	Three-Phase Currents
I_m	Current Linklists
$\hat{I}_m$	Reconstructed Current Linklists
p	Pole Pairs of IM
ω_0	Fundamental Frequency of Current
$z\omega_0$	Frequency of Reference Signal
D_m	DC Component of I_m
$\hat{D}_m$	Normilized DC Component of I_m
D^*_m	Filtered Normilized DC Component of I_m
$A_{m,h}$	h^{th} Fourier Series of I_m
$\hat{A}_{m,h}$	h^{th} Normilized Fourier Series of I_m
$A^*_{m,h}$	h_{th} Filtered Normilized Fourier Series of I_m
φ_m	Phase angle of Fourier Series
T	Current Period
T_{sp}	Current Sampling Period
L	Current Samples in a Period
k	Sampling Instant
H_m	Position of Down-to-Up Zero-Crossing Sample
N_1, N_2	Filters constant
ξ_1, ξ_0	Boundaries of Equality to 1 and 0

I. INTRODUCTION

THREE-PHASE VSIs are widely used in industrial applications due to their superior performance. Their health condition makes a vital contribution to the reliability of motor

drives. It is reported that the failure rate of power semiconductor takes up a large scale of the failure in motor drives, followed by capacitor and gate drives [1]. Consequently, lots of researches had been done on the fault diagnosis in three-phase VSIs to reach convenient maintenance and fault-tolerant in recent decades [2]–[6].

Generally, failures in three-phase VSIs can be divided into two categories: short-circuit and open-circuit. Short-circuit will cause overcurrent and has great damage to VSIs immediately [7]. Some positive protection is often taken, such as fault isolation by hardware design, as well as shut down the drive system immediately. The open-circuit fault is less destructive and causes system performance degraded by generating torque ripple and harmonics. The healthy components continue suffering overcurrent and overvoltage, which is extremely easy to cause secondary failure or even destroy the system if no positive actions are taken.

It should be noticed that the fault diagnosis consists of fault detection and fault location. Fault detection is applied to monitor system healthy conditions and provide safety strategies, such as shutting down the system. Fault location focuses on the position of fault after detection, which makes much sense to maintenance or switch to tolerant strategies.

The reported fault diagnosis methods in three-phase VSIs include two kinds: signal of component-based and signal of system-based. The former one uses the internal signal as diagnostic features by failure mechanism in the physical and electrical model of power component, such as collector-to-emitter voltage, the drain-to-source voltage, and gate-to-source voltage during the IGBT turn-on transient are used for healthy condition [8], [9]. Fast-detection, fair robustness to system disturbance and portability can be achieved by these methods. However, extra electrical circuit equipped with every power components will increase the cost and system volume, which limit their applications. System signal-based fault diagnosis methods are the most widely researched for feasible design and effective performance in recent years. They can be divided into two categories: voltage-based and current-based.

Voltage-based methods are proposed in [10]–[13], they may be further classified by the type of measured voltages-pole [10], phase [12], line or neutral voltage [13]. Fast diagnosis and fair robustness are the most advantages of these methods; however, extra sensors or electrical circuits are required, resulting in high cost. Recently, [14] proposes a voltage-based method by replacing the measured voltage with observed voltage. This method improves calculation, and no voltage sensor is required.

Current-based methods attract more attention because the diagnostic signals can be shared with the feedback current sensors. The diagnostic methods can be easily inserted into the controller as an independent subroutine. They can be further classified by currents-in $\alpha\beta$-axis, dq-axis, abc-axis. Park vector [15] and its modified approaches [16], [17] are the most classical diagnostic methods in $\alpha\beta$-axis. These approaches are not suitable for integration into the drive controller because they require complex pattern recognition algorithms and poor robustness. [18] proposes to divide three-phase currents into six stages and diagnosis in dq-axis, current in d-axis is used for fault detection and the current vector rotating angle is used to locate the faulty switches. Current-based diagnostic methods in abc-axis are the most widely researched, normalized DC current and its modified method are proposed in [19], [20]. They have some drawbacks when implemented in a closed-loop scheme and poor robustness to transients. [21] proposes load currents are applied to realize fault diagnosis with fuzzy classifier, [22] proposes to extract the fault features by the errors between the reference currents and the measured currents, [23], [24] proposes to use three-phase currents to describe the symmetry both in healthy and faulty conditions to realized fault detection and location, all these methods show fast diagnosis, fair robustness and acceptable tuning efforts. Besides, features extracted by signal processing and identified by pattern recognition, are also very popular as off-line techniques, such as discrete wavelet transform with support vector machine [25], fuzzy system [26], etc. These methods need a longer detection time and a complex implementation, compared with real-time methods, however, they have fair portability.

Lots of spectral analysis are used to locate the faulty transistor by analyzing the spectral distribution of phase currents [27], [28]. It should be noticed that these methods need extra signal processing hardware due to the complex calculation, which limits their application. In [19], the Fourier Series of currents are estimated by the motor rotating angle [19]; however, the estimation will be biased after fault occurrence, what is more, these methods are only available to a single open-circuit fault.

To overcome the complex calculation of traditional current spectral analysis methods. A simplified Fourier Series method is proposed, novel normalized DC and fundamental components are proposed for fault location for both single and multiple open-circuit faults. Two contributions are made in this paper, listed as follows.

1) A simplified Fourier series method is proposed by the product between reconstructed CLs and reference signals, and the computational complexity is $O(\log_2 L)$.
2) Novel normalized method for DC and fundamental components by simplified Fourier series are proposed to locate twenty-one transistor open-circuit, experimental results show high efficiency and merits.

The structure of this paper is as follows: Section II elaborates the proposed simplified Fourier series theory, including continuous and discrete systems, the concept of CDR. Section III concentrates the novel normalized method for DC and fundamental components and transistor open-circuit location. Section IV gives out experimental results, including the comparison of proposed simplified Fourier series method with FFT, fault location results and the comparison with previous spectral-analysis based methods. A conclusion is made in Section V.

II. SIMPLIFIED FOURIER SERIES IN VSI FED IM

The structure of three-phase VSI fed IM is showed in Fig.1, U_d is the input voltage of the drive system, C_1, C_2 are two symmetrical capacitors to eliminate high frequently harmonics of the supply voltage. T1, T2, T3, T4, T5, T6 are six power transistors, they are the core components of the drive system. D1, D2, D3, D4, D5, D6 are six stream diodes to avoid the impact caused by inductive rotating load. Three-phase currents (i_a, i_b, i_c), measured speed (ω), reference current in d-axis $(i_d{}^*)$ and reference speed are the inputs of control systems, pulse-width modulation signals are generated to switch their operation states between 'on' and 'off', alternately. As a result, DC to AC energy conversion is achieved.

In healthy conditions, three-phase currents are sinusoidal time series; their frequencies and amplitudes are the same, only with $2/3\pi$ phase difference between every two among them. In faulty conditions with open-loop control strategy, the phase currents of undamaged legs still keep the same as healthy condition, while the phase current of the damaged leg is distorted. However, in faulty condition with closed-loop control strategy, phase currents of undamaged legs will be spread by the phase current of the damaged leg for the feedback strategy. This paper focuses on transistor open-circuit fault location in VSI fed IM with FOC.

A. FOURIER SERIES IN CONTINUOUS SYSTEM

Three-phase output currents are periodic time series with period T, T is given as following Equation(1), Considering measurement error and system noise, reference speed is used in Equation (1).

$$T = \frac{30\omega^*}{9.55\pi p} \tag{1}$$

Three-phase currents can be represented by Fourier Series corresponding to a sum of harmonically related time series. The frequencies of these Fourier Series are integer multiples of the fundamental frequency ($\omega_0 = 2\pi/T$). These periodic Fourier Series are of the form,

$$I_m(t) = D_m + \sum_{h=1}^{+\infty} A_{m,h} sin(h\omega_0 t + \varphi_m) \tag{2}$$

$A_{m,h}$ are the amplitude of related exponential time series with frequency of $h\omega_0$. The integration of Equation (2) in a period is given,

$$\begin{aligned} \int_0^T I_m(t)dt = \int_0^T D_m dt + \\ A_{m,h} \sum_{h=1}^{+\infty} \int_0^T sin(h\omega_0 t + \varphi_m)dt \end{aligned} \tag{3}$$

$\forall h \in Z^+, \int_0^T sin(h\omega_0 t + \varphi_m)dt = 0$, D_m can be given as follows,

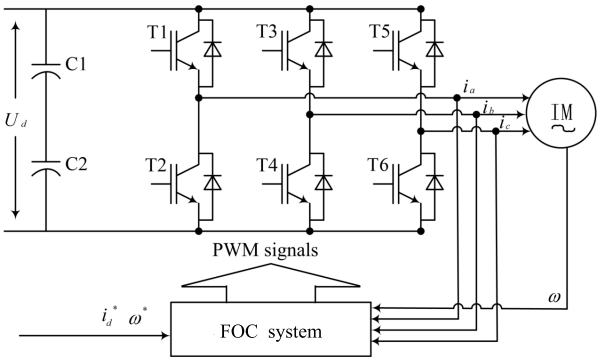

FIGURE 1. Structure of three-phase VSI fed IM.

$$D_m = \frac{1}{T} \int_0^T I_m(t)dt \tag{4}$$

Equation (2) is multiplied by a reference signal, whose frequency is $z\omega_0$, phase angle is the same as original signal, there is,

$$\begin{aligned} I_m(t)sin(z\omega_0 t + \varphi_m) = D_m sin(z\omega_0 t + \varphi_m) + \\ \sum_{h=1}^{+\infty} A_{m,h} sin(h\omega_0 t + \varphi_m) sin(z\omega_0 t + \varphi_m) \end{aligned} \tag{5}$$

The integration of Equation (5) in a period is given,

$$\begin{aligned} \int_0^T I_m(t)sin(z\omega_0 t + \varphi_m)dt = D_m \int_0^T sin(z\omega_0 t + \varphi_m)dt \\ + A_{m,h} \int_0^T \sum_{h=1}^{+\infty} sin(h\omega_0 t + \varphi_m) sin(z\omega_0 t + \varphi_m)dt \end{aligned} \tag{6}$$

The orthogonality of trigonometric functions has a characteristic showed as Equation (7),

$$\begin{aligned} \int_0^T sin(h\omega_0 t) sin(z\omega_0 t)dt = 0 \\ h \neq z \end{aligned} \tag{7}$$

Substituting Equation (7) in (6) and simplifying yields,

$$\begin{aligned} \int_0^T I_m(t)sin(z\omega_0 t + \varphi_m)dt = \\ A_{m,z} \int_0^T sin(z\omega_0 t + \varphi_m) sin(z\omega_0 t + \varphi_m)dt \end{aligned} \tag{8}$$

$A_{m,z}$ can be calculated as Equation (8),

$$A_{m,z} = \frac{\int_0^T I_m(t)sin(z\omega_0 t + \varphi_m)dt}{\int_0^T sin^2(z\omega_0 t + \varphi_m)dt} \tag{9}$$

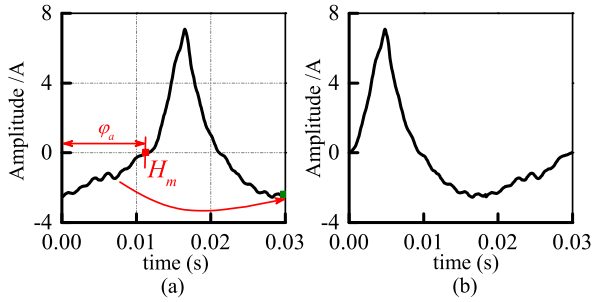

FIGURE 2. Illustration of CDR in phase-a When T1 open-circuit fault occurs. (a) original phase current. (b) reconstructed phase current.

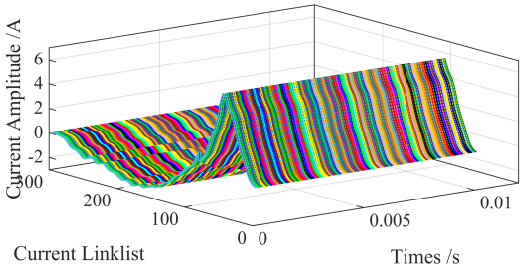

FIGURE 3. Simulation Results of reconstructed CL in phase-a when T1 open-circuit fault occurs within 0.01s.

B. FOURIER SERIES IN DISCRETE SYSTEM

In discrete system, three-phase currents in a period are composed of L samples, named CLs, their length is given as following.

$$L = \frac{T}{T_{sp}} \tag{10}$$

In k instant, t is defined as the ending position of CL,

$$t = k - L + 1 \tag{11}$$

Three phase CLs are given,

$$I_m = \left| i_m(t), i_m(t+1), \cdots, i_m(k) \right| \tag{12}$$

a: DC component

$$D_m(k) = \frac{1}{L} \sum_{j=t}^{k} I_m(j) \tag{13}$$

b: AC component

$$A_{m,z}(k) = \frac{\sum_{j=t}^{L} I_m(j) sin(\frac{j}{L} T z \omega_0 + \varphi_m(k))}{\sum_{j=t}^{k} sin^2(\frac{j}{L} T z \omega_0 + \varphi_m(k))} \tag{14}$$

DC component can be easily calculated. However, the real-time calculation of AC component is challenging because $\varphi_{a,b,c}(k)$ are uncertain variables. In every sampling instant, $\varphi_a \neq \varphi_b \neq \varphi_c$, what's more, in any two sampling instants during a period, there is $\varphi_m(p) \neq \varphi_m(g)$, where $p, g \in [t, t+1, \cdots, k]$.

In order to eliminate the difference between φ_a, φ_b, φ_c and the difference in any two sampling instants during a period $\varphi_m(p)$, $\varphi_m(g)$, a CDR algorithm is proposed.

C. CDR AND SIMPLIFIED FOURIER SERIES

There are two ZCSs in every CL, one is up-to-down ZCS, the other one is down-to-up ZCS. The positions of down-to-up ZCS in CLs I_m are marked as H_m. In , all samples before H_m are removed back to the last sample $i_m(k)$ to form $\hat{I}_m$. The CDR process of phase-a when T4 fails is showed as

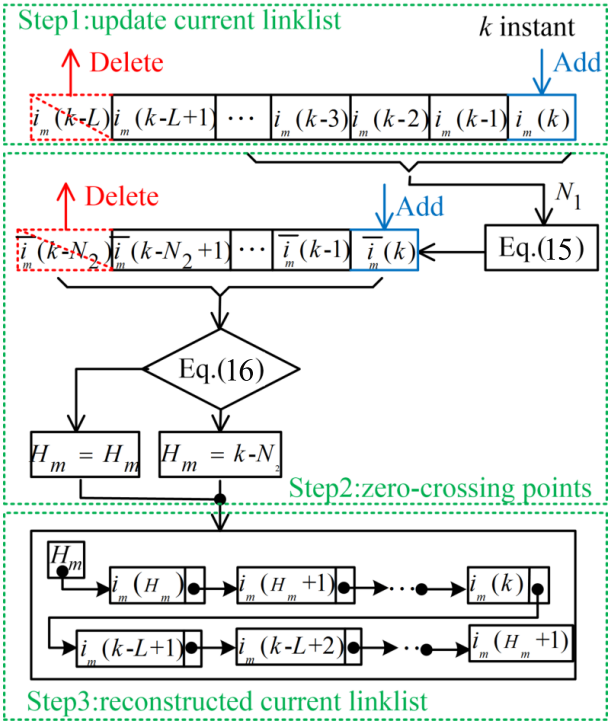

FIGURE 4. Algorithm flowchart of down-to-up ZCS position calculation in k instant.

subplot (a) in Fig.2, and the reconstructed result is showed in subplot (b) in Fig. 2. Compared with the original CLs, in the reconstructed CLs, only the order of the samples changes.

Here, assuming that the phase angle of ZCS in every instant is approximated to φ_m, then φ_a is showed in Fig. 2, the reconstructed CLs are nearly the same with $\varphi_m \approx 0$, shown in Fig. 3.

Fig.4 shows the flowchart of CDR in k instant, including three steps:

1) Update the CL by adding the new sample and deleting the ending sample.
2) Calculate H_m.
3) Update $\hat{I}_m$.

Current harmonics and system noise will cause fluctuation near ZCS, which has a negative influence on the calculation of H_m. Here, a ZCS calculation algorithm is given. Three-

phase currents are firstly filtered, as following,

$$\bar{i}_m(k) = \frac{\sum_{j=k-N_1+1}^{k} I_m(j)}{N_1} \tag{15}$$

Where N_1 is a constant. Secondly, $\forall j = k - N_2, v \in [k - N_2 + 1, k - N_2 + 2, \cdots, k]$, if

$$\begin{cases} I_m(j) < 0 \\ I_m(v) \geqslant 0 \end{cases} \tag{16}$$

Then, $H_m = k - N_2$. The proposed ZCS calculation algorithm has a short delay-time with $N_2 T_{sp}$ because $I_m(k-N_2)$ is checked in k instant. If Equation (16) is established, H_m is replaced by the position of the new down-to-up ZCS $k - N_2$, if Equation (65) is not established, H_m shifts left because I_m updates. As a result, in every instant, the original CLs I_m are replaced by reconstructed CLs $\hat{I}_m$, $\varphi_a(k) = \varphi_b(k) = \varphi_c(k)$, The proposed simplified Fourier series can be presented as following.

$$A_{m,z}(k) = \frac{\sum_{j=t}^{L} \hat{I}_m(j) sin(\frac{j}{L} T z \omega_0)}{\sum_{j=t}^{k} sin^2(\frac{j}{L} T z \omega_0)} \tag{17}$$

III. PROPOSED FAULT LOCATION METHOD

The accuracy of harmonics amplitude and phase errors in three-phase currents can all be controlled within 5% in healthy condition. When the transistor open-circuit fault occurs, Fourier series of three-phase currents change with high DC component and harmonics. A different open-circuit fault will lead to different harmonics distributions in three-phase currents. Compared with FFT or other improved methods, the proposed simplified Fourier series can be easily implemented with low calculation consumption. VSI transistor open-circuit fault location method is proposed by analyzing the Fourier series.

A. THREE PHASE CURRENT SPECTRAL ANALYSIS

In healthy conditions, the fundamental series accounts for the vast majority in three-phase currents. In faulty condition, the Fourier Series associated with a frequency of $z\omega_0$ increase. Here, twenty-one single and multiple open-circuit faults are divided into four categories: single open circuit fault, multiple open-circuit fault in the same leg, multiple open-circuit fault both on the upper or on the lower of different legs, multiple open-circuit fault that one is on the upper and the other one is on the lower of different legs, respectively. Fourier series distributions of three-phase currents are different among four categories, and they are the same within categories.

In FFT, the amplitudes $(D_m, A_{m,z})$ or percentages $(\overline{D}_m, \overline{A}_{m,z})$ of DC and AC components are used for fault diagnosis. Where $\overline{D}_m$, $\overline{A}_{m,z}$ are defined as following,

$$\begin{cases} \overline{D}_m = \dfrac{|D_m|}{|D_m| + \sum_{z=1}^{L/2} |A_{m,z}|} \\ \overline{A}_{m,z} = \dfrac{|A_{m,z}|}{|D_m| + \sum_{z=1}^{L/2} |A_{m,z}|} \end{cases} \tag{18}$$

These features focus on the characteristics without considering the interaction. However, in the closed-loop system, transistor open-circuit fault on the faulty leg will propagate to healthy legs. Hence, a novel normalized method for DC and AC components is proposed by taken into the interaction. AC components are divided by the maximum amplitude of fundamental components; DC components are divided by the maximum absolute value of the sum of CLs, shown as follows.

$$\begin{gathered} A_{max,1} = max(|A_{a,1}|, |A_{b,1}|, |A_{c,1}|) \\ D_{max} = max(\sum_{j=t}^{k} |D_a(j)|, \sum_{j=t}^{k} |D_b|, \sum_{j=t}^{k} |D_c|) \\ \begin{cases} \hat{D}_m = \dfrac{D_m}{D_{max}} \\ \hat{A}_{m,z} = \dfrac{A_{m,z}}{A_{max,1}} \end{cases} \end{gathered} \tag{19}$$

Substituting Equation (17) in (19) and simplifying yields, normalized AC components can be online calculated by (20), where $\hat{I}_v(v = a, b, c)$ is the CL of $A_{max,1}$.

$$\hat{A}_{m,z} = \frac{\sum_{j=t}^{L} \hat{I}_m(j) sin(z\frac{2\pi j}{L})}{\sum_{j=t}^{L} \hat{I}_v(j) sin(\frac{2\pi j}{L})} \tag{20}$$

Table 1 gives the FFT and proposed normalized Fourier Series of currents under 30% IM RLT at 1000r/min, these data are from experimental board and off-line calculated by Matlab. The motor parameters are listed in Table 2. The first part in Table 1 gives $(\overline{D}_m, \overline{A}_{m,z}(z = 1, 2, 3, 4, 5))$ calculated by Equation (18). The second part in Table 1 are normalized Fourier series $|\hat{D}_m|, |\hat{A}_{m,z}|(z = 1, 2, 3, 4, 5)$ calculated by Equation (19). Compared with the FFT, features are much more recognizable in the proposed normalized Fourier Series.

1) The normalized fundamental components of healthy legs are larger than that of faulty legs.
2) The normalized DC components are not equal to zero in fault legs.

The operation principle of VSI is applied to explain the mentioned features. Fig.5 (a),(b) shows the negative and positive current flows in a faulty leg with lower transistor T_{k+1} open-circuit, T_k is turned on and off alternatively. When $i_m > 0$, the current flows from DC-link to IM in two cases, one case is through T_k directly if it is turned on, another case is through V_{k+1} during the dead-time interval

TABLE 1. Traditional and Proposed Normalized Fourier Series of Three Phase Currents Calculated by FFT

Fourier series	T4 open failure			T3T4 open failure			T4T5 open failure			T4T6 open failure		
	phase-a	phase-b	phase-c	phase-a	phase-b	phase-c	phase-a	phase-b	phase-c	phase-a	phase-b	phase-c
$\overline{D}_m(\%)$	2.65	37.61	21.10	1.59	20.84	1.09	0.90	34.70	36.91	28.73	19.57	23.35
$\overline{A}_{m,1}(\%)$	38.96	27.99	39.02	51.42	5.07	51.86	40.18	24.98	27.94	25.89	21.12	20.03
$\overline{A}_{m,2}(\%)$	18.22	9.42	12.13	3.07	5.85	3.09	21.07	7.01	12.12	16.49	18.36	13.87
$\overline{A}_{m,3}(\%)$	11.13	4.01	8.49	19.38	6.93	19.48	4.85	3.42	1.35	7.55	11.62	9.51
$\overline{A}_{m,4}(\%)$	7.22	3.82	4.23	1.80	5.70	1.93	2.72	0.89	2.97	3.87	6.88	7.89
$\overline{A}_{m,5}(\%)$	5.54	2.23	3.43	7.44	3.85	7.41	0.77	0.75	0.90	2.38	5.53	5.26
$\lvert\hat{D}_m\rvert$	0.0584	0.5991	0.5407	0.1192	0.0108	0.1084	0.0224	1.0656	1.0432	1.1353	0.6553	0.4800
$\lvert\hat{A}_{m,1}\rvert$	0.8594	0.4460	1	0.9994	0.0016	1	1	0.7672	0.7897	1	0.7010	0.4080
$\lvert\hat{A}_{m,2}\rvert$	0.4019	0.1510	0.3109	0.0660	0.0046	0.0657	0.5244	0.2153	0.3425	0.6024	0.5990	0.2726
$\lvert\hat{A}_{m,3}\rvert$	0.2456	0.0640	0.2176	0.3568	0.0041	0.3547	0.1207	0.1049	0.0381	0.2590	0.3671	0.1857
$\lvert\hat{A}_{m,4}\rvert$	0.1593	0.0609	0.1085	0.0445	0.0013	0.0459	0.0677	0.0273	0.0838	0.1158	0.2089	0.1530
$\lvert\hat{A}_{m,5}\rvert$	0.1223	0.0356	0.0880	0.1166	0.0028	0.1139	0.0192	0.0231	0.0254	0.0679	0.1623	0.0944

TABLE 2. Motor Parameters

Parameters	Values	Parameters	Values
Rotor resistance	2.718Ω	Rated Power	2.2kW
Rotor leakage inductance	10.33mH	Frequency	50Hz
Magnetizing inductance	319.7mH	Poles	4
Stator leakage inductance	10.33mH	RLT	14N · m
Stator leakage resistance	2.804Ω	flux-leakage	0.6Wb

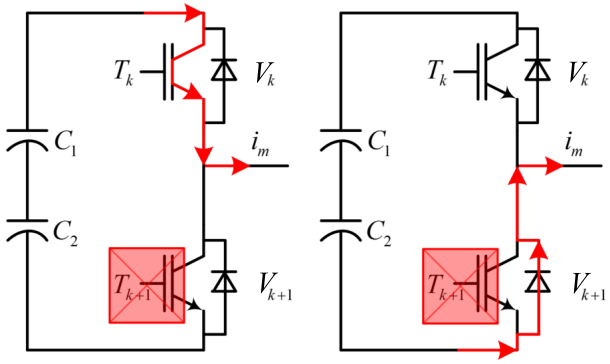

FIGURE 5. Illustration of Current flow when the lower transistor is open-circuit, (a) output current is positive, (b) output current is negative.

that is applied to prevent short-circuit fault. T_{k+1} makes no sense when $i_m > 0$. When $i_m < 0$, the current flows out of IM in two cases, one case is through T_{k+1} if it is turned on. However, this circuit can not be conducted when T_{k+1} open-circuit fault occurs. Another case is through V_k during the dead-time interval. The interval is so short that it can be ignored. Consequently, T_{k+1} open-circuit fault will cause the $i_m \geq 0$, leading to a DC component with large positive value. Similarly, available T_k open-circuit fault leads to a DC component with a large negative value.

The absolute values of $\hat{A}_{m,1}$ represent the correlation, transistor open-circuit fault breaks the modulation mechanism, leading to smaller fundamental component. $\hat{A}_{m,1}$ also reflect the symmetry of the topology, when leg-b is broken (T4 fails or T3 & T4 fail), leg-a and leg-c are symmetrical, and they are asymmetrical with leg-c. $|\hat{A}_{a,1}| \approx |\hat{A}_{c,1}| > |\hat{A}_{b,1}|$.

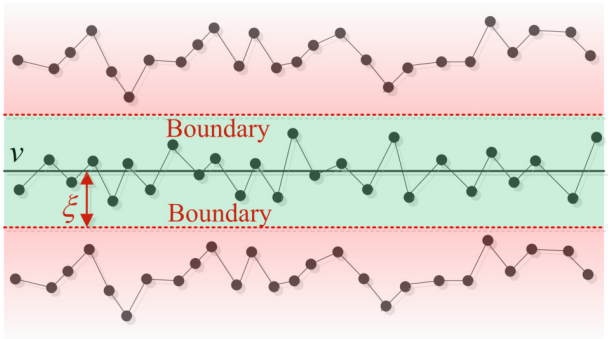

FIGURE 6. Illustration of Equality to a constant.

B. PROPOSED FAULT LOCATION METHOD

Fundamental components of three phase currents are used to distinguish faulty leg from healthy legs, DC components are used to locate the faulty transistor. Assuming that three legs are leg-m, leg-n, leg-l, $m, n, l = a, b, c, m \neq n \neq l$,

For one faulty leg, such as leg -m: absolute values of normalized fundamental components in phase currents will be: $|\hat{A}_{m,1}| < 1|$, $|\hat{A}_{n,1}|, |\hat{A}_{l,1}|$ are closed to 1. Specially, if the faulty transistor is on the upper, $D_m < 0$; if the faulty transistor is on the lower, $\hat{D}_m > 0$; if both the lower and the upper transistors are faulty, $\hat{D}_m = 0$.

For two faulty legs, such as leg-m and leg-n, absolute values of normalized fundamental components in phase current will be: $|\hat{A}_{m,1}| < 1, |\hat{A}_{n,1}| < 1$, $|\hat{A}_{l,1}| = 1$. Specially, $\hat{D}_m > 0, \hat{D}_n > 0$ indicates both two faulty transistors are on the lower of the legs, $\hat{D}_m < 0, \hat{D}_n < 0$ indicates both two faulty transistors are on the upper of the legs, $\hat{D}_m > 0, \hat{D}_n < 0$ indicates the upper transistor of leg-m and the lower transistor of leg-n are faulty, $\hat{D}_m < 0, \hat{D}_n > 0$ indicates the upper transistor of leg-m and the lower transistor of leg-n are faulty.

Considering system noise and measurement errors, two symmetrical boundaries near predefined constant are set as Fig.6, where the predefined constant is v, the distance between boundaries is 2ξ. If a variable is inside two boundaries, shown as the light green zone, it is considered equal to v.

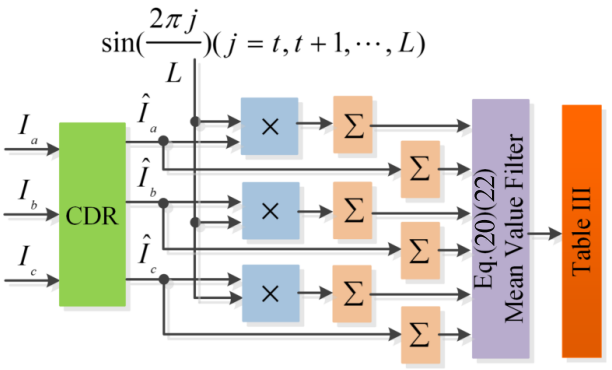

FIGURE 7. Algorithm flowchart of Transistor Open-Circuit Fault Location.

Otherwise, if a variable is larger than the upper boundary, it is considered larger than the v, if a variable is smaller than the lower boundary, it is considered smaller than the v, the criterion is given as,

$$F = \hat{D}_m, \hat{A}_{m,1}$$
$$\begin{cases} F = v, & |F - v| \le \xi \\ F > v, & F - v > \xi \\ F < v, & v - F < \xi \end{cases} \tag{21}$$

Based on the analysis above, a fault location table to locate twenty-one single and multiple open-circuit faults are proposed as Table 3. Where $\times$ means a does not care condition, D_m^*, A_m^* are filtered values of $\hat{D}_m, \hat{A}_m$, given as,

$$\begin{cases} D_m^*(k) = \dfrac{1}{L}\displaystyle\sum_{j=t}^{k} \hat{D}_m(j) \\ A_m^*(k) = \dfrac{1}{L}\displaystyle\sum_{j=t}^{k} \hat{A}_m(j) \end{cases} \tag{22}$$

Absolute values of $A_{m,1}^*$ are applied to locate faulty legs, sign, and values of D_m^* are applied to locate the position of the faulty transistor. The flowchart of the proposed fault location algorithm is given as Fig.7, which includes three steps:

1) CDR to eliminate $\varphi_m(k)$
2) Normalized DC and fundamental components calculation, equation(17)-(22)
3) Look up table 3

C. TUNING EFFORT

An important property of diagnosis algorithm is low tuning effort. The proposed fault location method needs four parameters, N_1, N_2, $\xi_0$and ξ_1. N_1, N_2 are two constants applied to ZCS calculation, N_1 is a filter constant, it makes sense when the currents contain high harmonics. N_2 is applied to search for the position of ZCS. It plays an important role in the proposed algorithm. In fact, the number of positive samples on the right of ZCS is smaller than $L/2$. Hence, the upper limit of N_2 is $L/2$, and N_2 is suggested to set as large enough to improve the accuracy of CDR. ξ_0, ξ_1 are applied to measure the equivalent relationship with 0, 1, respectively. The value ranges of these four parameters are shown in Table IV, where large efficient value ranges show low tuning effort.

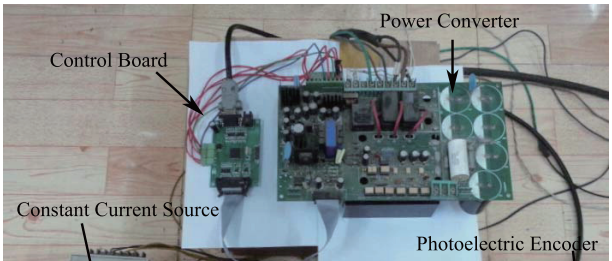

FIGURE 8. Experimental setup.

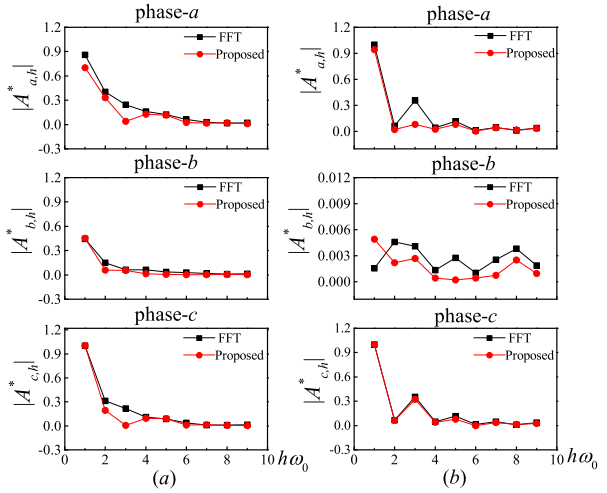

FIGURE 9. Comparison of proposed real-time Fourier series approximated algorithm with FFT. (a) T1 fails, (b) T3 and T4 fail.

IV. EXPERIMENTAL RESULTS

The following analyses are based entirely on the experimental results since they give an understandable presentation of the algorithm performance in the presence of nonideal properties, such as model uncertainty, measurement noise, dead-time effects, etc. FOC with SVPWM was the control algorithm in the experiment. Some indices were presented to evaluate the performance of the proposed fault location method, such as location time, effectiveness, etc. Four typical faulty operating conditions were investigated. All kinds of

TABLE 3. Proposed Transistor Open-Circuit Fault Location Table

Normalized DC Component			Normalized Fundamental Component			Faulty Transistor	Fault Type
$D_a^*=0$	$D_b^*=0$	$D_c^*=0$	$\lvert A_{a,1}^*\rvert<1$	$\lvert A_{b,1}^*\rvert=1$	$\lvert A_{c,1}^*\rvert=1$	T1T2	1
$D_a^*=0$	$D_b^*=0$	$D_c^*=0$	$\lvert A_{a,1}^*\rvert=1$	$\lvert A_{b,1}^*\rvert<1$	$\lvert A_{c,1}^*\rvert=1$	T3T4	2
$D_a^*=0$	$D_b^*=0$	$D_c^*=0$	$\lvert A_{a,1}^*\rvert=1$	$\lvert A_{a,1}^*\rvert=1$	$\lvert A_{c,1}^*\rvert<1$	T5T6	3
$D_a^*>0$	$\times$	$\times$	$\lvert A_{a,1}^*\rvert<1$	$\lvert A_{b,1}^*\rvert=1$	$\lvert A_{c,1}^*\rvert=1$	T2	4
$D_a^*<0$	$\times$	$\times$	$\lvert A_{a,1}^*\rvert<1$	$\lvert A_{b,1}^*\rvert=1$	$\lvert A_{c,1}^*\rvert=1$	T1	5
$\times$	$\hat{D}_b>0$	$\times$	$\lvert A_{a,1}^*\rvert=1$	$\lvert A_{b,1}^*\rvert<1$	$\lvert A_{c,1}^*\rvert=1$	T4	6
$\times$	$D_b^*<0$	$\times$	$\lvert A_{a,1}^*\rvert=1$	$\lvert A_{b,1}^*\rvert<1$	$\lvert A_{c,1}^*\rvert=1$	T3	7
$\times$	$\times$	$D_c^*>0$	$\lvert A_{a,1}^*\rvert=1$	$\lvert A_{b,1}^*\rvert=1$	$\lvert A_{c,1}^*\rvert<1$	T6	8
$\times$	$\times$	$D_c^*<0$	$\lvert A_{a,1}^*\rvert=1$	$\lvert A_{b,1}^*\rvert=1$	$\lvert A_{c,1}^*\rvert<1$	T5	9
$D_a^*>0$	$D_b^*>0$	$\lvert D_c^*\rvert=\lvert D_a^*\rvert+\lvert D_b^*\rvert$	$\lvert A_{a,1}^*\rvert<1$	$\lvert A_{c,1}^*\rvert<1$	$\lvert A_{c,1}^*\rvert=1$	T2T4	10
$D_a^*<0$	$D_b^*<0$	$\lvert D_c^*\rvert=\lvert D_a^*\rvert+\lvert D_b^*\rvert$	$\lvert A_{a,1}^*\rvert<1$	$\lvert A_{c,1}^*\rvert<1$	$\lvert A_{c,1}^*\rvert=1$	T1T3	11
$D_a^*>0$	$\lvert D_b^*\rvert=\lvert D_a^*\rvert+\lvert D_c^*\rvert$	$D_c^*>0$	$\lvert A_{b,1}^*\rvert<1$	$\lvert A_{b,1}^*\rvert=1$	$\lvert A_{c,1}^*\rvert<1$	T2T6	12
$D_a^*<0$	$\lvert D_b^*\rvert=\lvert D_a^*\rvert+\lvert D_c^*\rvert$	$D_c^*<0$	$\lvert A_{b,1}^*\rvert<1$	$\lvert A_{b,1}^*\rvert=1$	$\lvert A_{c,1}^*\rvert<1$	T1T5	13
$\lvert D_a^*\rvert=\lvert D_b^*\rvert+\lvert D_c^*\rvert$	$D_b^*>0$	$D_c^*>0$	$\lvert A_{a,1}^*\rvert=1$	$\lvert A_{b,1}^*\rvert<1$	$\lvert A_{c,1}^*\rvert<1$	T4T6	14
$\lvert D_a^*\rvert=\lvert D_b^*\rvert+\lvert D_c^*\rvert$	$D_b^*<0$	$D_c^*>0$	$\lvert A_{a,1}^*\rvert=1$	$\times$	$\times$	T3T5	15
$D_a^*=1$	$D_b^*=-1$	$\lvert D_c^*\rvert=\lvert\lvert D_a^*\rvert-\lvert D_b^*\rvert\rvert$	$\times$	$\times$	$\lvert\hat{A}_{c,1}\rvert=1$	T2T3	16
$D_a^*=-1$	$D_b^*=1$	$\lvert D_c^*\rvert=\lvert\lvert D_a^*\rvert-\lvert D_b^*\rvert\rvert$	$\times$	$\times$	$\lvert A_{c,1}^*\rvert=1$	T1T4	17
$D_a^*=1$	$\lvert D_b^*\rvert=\lvert\lvert D_a^*\rvert-\lvert D_c^*\rvert\rvert$	$D_c^*=-1$	$\times$	$\lvert A_{b,1}^*\rvert=1$	$\times$	T2T5	18
$D_a^*=-1$	$\lvert D_b^*\rvert=\lvert\lvert D_a^*\rvert-\lvert D_c^*\rvert\rvert$	$D_c^*=1$	$\times$	$\lvert A_{b,1}^*\rvert=1$	$\times$	T1T6	19
$\lvert D_a^*\rvert=\lvert\lvert D_b^*\rvert-\lvert D_c^*\rvert\rvert$	$D_b^*=1$	$D_c^*=-1$	$\lvert A_{a,1}^*\rvert=1$	$\times$	$\times$	T4T5	20
$\lvert D_a^*\rvert=\lvert\lvert D_b^*\rvert-\lvert D_c^*\rvert\rvert$	$D_b^*=-1$	$D_c^*=1$	$\lvert A_{a,1}^*\rvert=1$	$\times$	$\times$	T3T6	21

TABLE 4. Efficient Value Ranges of Parameters In Proposed Algorithm

Parameters	N_1	N_2	ξ_0	ξ_1
value ranges	4-10	$L/20-L/3$	0.1-0.3	0.1-0.3

transistor open-circuit faults were performed by inhibiting their respective gate signals while keeping the bypass diode still connected. The experimental results are presented by signal $FaultType$.

The experimental validation of the proposed fault diagnosis method was implemented in a TMS320F2806 board. The experimental setup was shown in Fig.8, consisting of a $2.2kW$ squirrel-cage IM with $380V$ rated voltage, $4.9A$ rated current, a power converter with a switching frequency of $20kHz$ and the dead time of $3.2\mu s$, a control board, a magnetic power brake, and a constant current source. The parameters of IM were listed in Table 2. The thresholds N_1, N_2 for CDR were set as 4, 50, respectively. The thresholds ξ_0 was set 0.2, ξ_1 was set 0.25.

A. COMPARISON OF PROPOSED FOURIER SERIES APPROXIMATED ALGORITHM WITH FFT

The comparison of proposed online simplified Fourier series approximated algorithm with offline FFT algorithm for normalized DC and AC components were made when T1 and T1T4 fault occur at a reference speed of 1000rpm with 30% IM RLT, showed as subfigure (a) and (b) of Fig.9, respectively. The absolute values of normalized ${D_m}^*$, ${A_{m,h}}^*$ $(h=1,2,\ldots,9)$ coincide with that of FFT besides parts of 3^{rd} harmonics, the efficiency of the assumption to eliminate $\varphi_m(k)$ by CDR is proved.

B. RESULTS OF PROPOSED FAULT LOCATION ALGORITHM

Fig.10 (a),(b),(c) present three-phase reconstructed CLs in every sampling instant for single open-circuit fault in T4 at 1000rpm with 30% RLT, the left subfigures are the 3-D view of the reconstructed CLs during 0.4s, the color of bar represents the amplitude, the right subfigures are the side view of reconstructed CLs during 0.4s. The number of current samples during a period is 300, calculated by Equation (10), representing the length of CLs, the fault occurs at 0.28s. All phase differences are eliminated in three-phase currents in every instant. For $\forall p, g(p\neq g)$, there is $\varphi_m(p)=\varphi_m(g)$, showed in three subfigures respectively.There is $\varphi_a(k)=\varphi_b(k)=\varphi_c(k)$, showed among three subfigures, the phase angles of three-phase CLs nearly coincide. In every phase, reconstructed CL has two states, healthy states, and faulty states, shown as the side view subfigures.

Fig.11 presents the experimental results for a single fault in T6, under 30% IM RLT and 500r/min reference speed. Torque ripples and distorted currents occur after fault, showed as subfigure 1, 2. The normalized DC and fundamental components of the simplified Fourier series by the proposed method are presented in subfigure 3, 4, respectively. Subfigure 5 gives out the fault location result.

In healthy conditions, three-phase currents are sinusoidal, $|\hat{A}_{m,1}|=1$, normalized DC components, and harmonics are nearly equal to zero. After T6 fails, DC component of leg-c, $\hat{D}_c$ raises. Due to $\hat{D}_a+\hat{D}_b+\hat{D}_c=0$, DC components will also exist in healthy legs. Meanwhile, the fundamental component is nearly equal to 1 in the healthy leg, while it is smaller than 1 in the faulty leg. In subfigure 4, $\hat{A}_{a,1}, \hat{A}_{b,1}$ are inside the boundaries made up by ξ_1, while $\hat{A}_{c,1}$ are

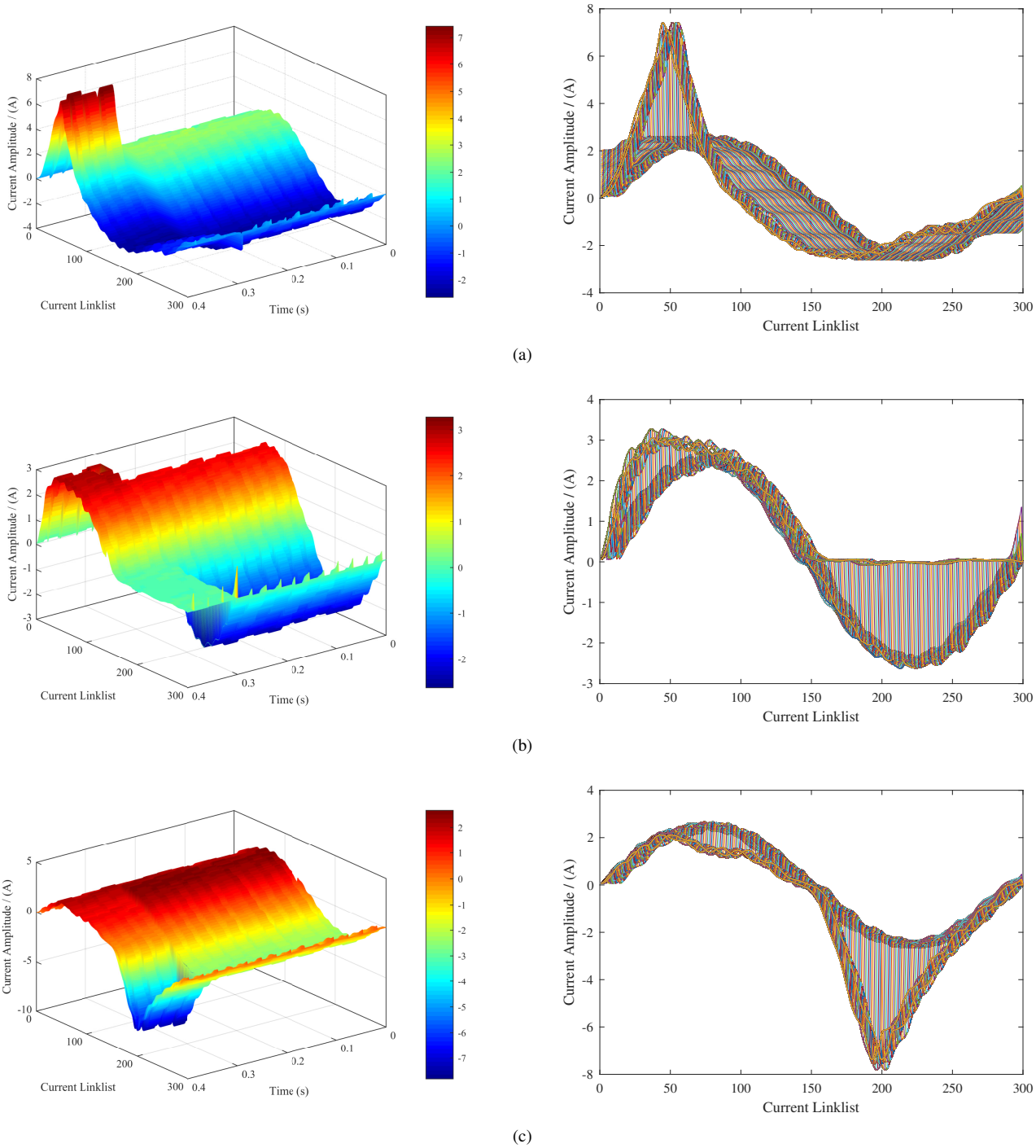

FIGURE 10. Three phase reconstructed CLs both in healthy condition and faulty condition. (a) CLs of phase-a, left: 3D view, right: side view. (b) CLs of phase-b, left: 3D view, right: side view. (c) CLs of phase-c, left: 3D view, right side view.

outside ξ_1, which indicates leg-c is faulty. In subfigure 3, $\hat{D}_c$ is larger than ξ_0, the DC component in phase current of leg-c is positive, which indicates the lower transistor is faulty. Combining the results of subfigure 3 and 4, the fault can be located to T6 by looking up table 3, the location flag $FaultType$ raises to 8, showed in subfigure 5.

Fig. 12 presents the experimental results for multiple open-circuit faults, under 30% IM RLT and assuming a reference speed of 1000r/min. Motor measured speed and three-phase currents are showed in subfigure 1, 2, respectively. Normalized DC, fundamental and $2^{th}-8^{th}$ components are given in subfigure 3-4. In subfigure 4, $|A^*_{a,1}| = |A^*_{c,1}| = 1$, $A^*_{b,1}$ are smaller than ξ_1, which indicates leg-b is faulty. In subfigure 3, D^*_b is inside the boundaries made up by ξ_0 before and after

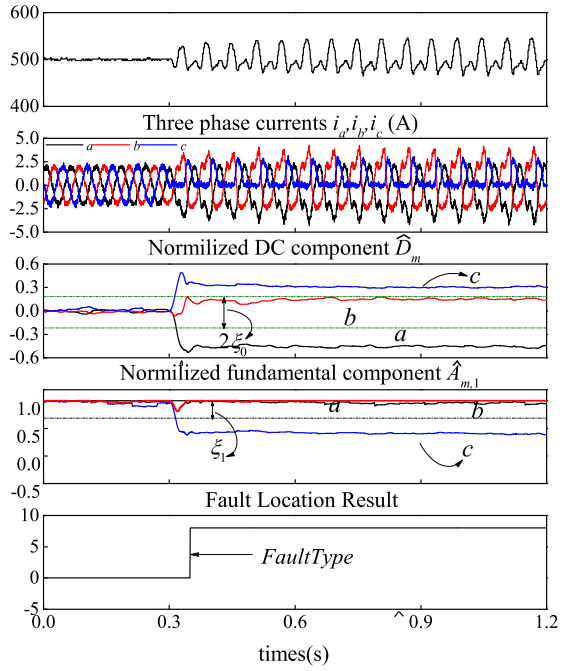

FIGURE 11. Experimental results concerning the time-domain waveforms of motor speed, three phase currents, real-time Normalized DC, AC components and fault location flag for a single open-circuit fault in T6.

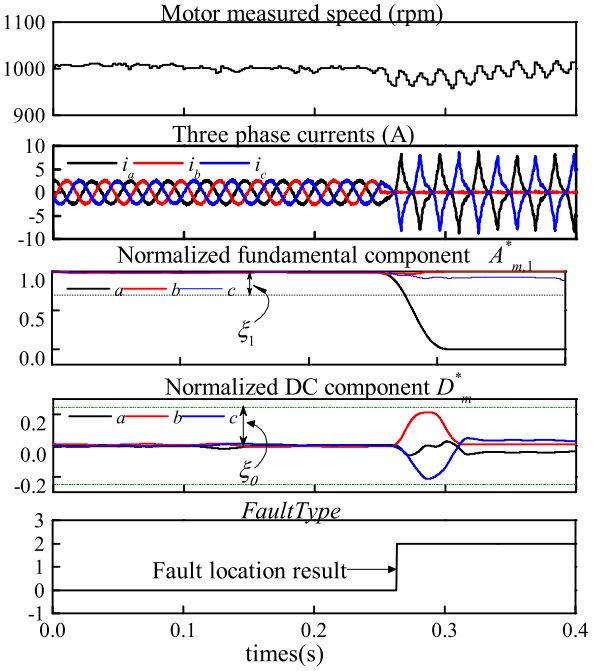

FIGURE 13. Experimental results concerning the time-domain waveforms of motor speed, three phase currents, real-time Normalized DC, AC components and fault location flag for multiple open-circuit fault in T3 and T4.

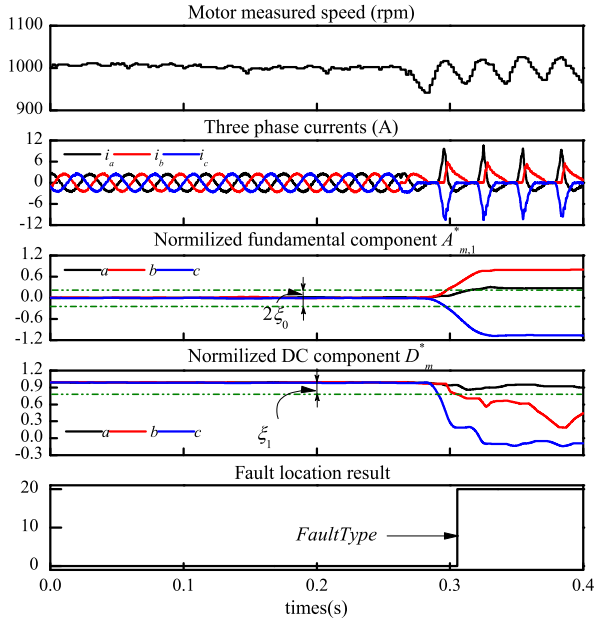

FIGURE 12. Experimental results concerning the time-domain waveform of motor speed, three phase currents, real-time Normalized DC, fundamental components, and fault location flag for multiple open-circuit fault in T4 and T5.

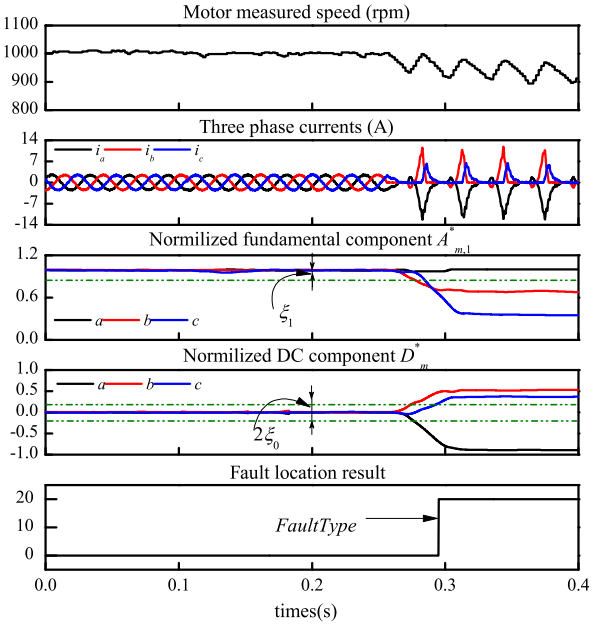

FIGURE 14. Experimental results concerning the time-domain waveform of motor speed, three phase currents, real-time Normalized DC, fundamental components, and fault location flag for multiple open-circuit fault in T4 and T6.

fault occurrence, which indicates both the upper and lower transistors are faulty. As a result, the open-circuit fault can be located in T3 and T4. The location flag is showed in subfigure 5.

Fig. 13 presents the experimental results for multiple open-circuit fault at 0.28s, under 30% IM RLT and assuming a reference speed of 1000r/min. Motor measured speed and three phase currents are showed in subfigure 1, 2, respectively. Real-time calculated normalized DC, fundamental components are showed in subfigure 3, 4, respectively. In subfigure

TABLE 5. Comparison with Previous VSI Fault Location Methods

Fault Location Methods	Calculation Consume	Efficiency	Cost	Implementation	Tuning efforts
Fourier Transform of Bus Current [27]	O($L \log L$))	single and multiple	low	high	medium
FFT of Output Voltage [28]	O($L \log L$))	single	high	high	medium
Normalized DC Current Method [19], [20]	O(L)	single	low	low	low
Proposed Method	O($\log_2 L$)	single and multiple	low	low	low

4, only $A^*_{a,1}$ is inside ξ_1, $A^*_{b,1}, A^*_{c,1}$ are outside the boundaries made up by ξ_1, $|A^*_{a,1}| = 1$, $|A^*_{b,1}|, |A^*_{c,1}| < 1$, which indicates phase-$a$ is healthy. In subfigure 3, $D^*_b > 0, D^*_c < 0$ and $|D^*_a| = ||D^*_b| - |D^*_c||$, which indicates the lower transistor of leg-b and the upper transistor of leg-c are broken. As a result, fault is located to T4 and T5, showed in subfigure 5.

Fig. 14 presents the experimental results for multiple open-circuit fault at 0.27s, under 30% IM RLT and assuming a reference speed of 1000r/min. Motor measured speed and three phase currents are showed in subfigure 1, 2, respectively. Real-time calculated normalized DC, fundamental components are showed in subfigure 3, 4, respectively. In subfigure 4, only $A^*_{a,1}$ is inside ξ_1, $A^*_{b,1}, A^*_{c,1}$ are outside the boundaries made up by ξ_1, $|A^*_{a,1}| = 1$, $|A^*_{b,1}|, |A^*_{c,1}| < 1$, which indicates phase-$a$ is healthy. In subfigure 3, $D^*_b > 0, D^*_c > 0$ and $|D^*_a| = |D^*_b| + |D^*_c|$, which indicates the lower transistors of leg-b and leg-c are broken. As a result, fault is located to T4 and T6, showed in subfigure 5.

C. COMPARISON WITH PREVIOUS SPECTRAL ANALYSIS BASED VSI FAULT LOCATION METHODS

The performance of the proposed transistor open-circuit fault location method is compared with previous methods in calculation consume, efficiency, cost, implementation, and tuning effort. [27] and the proposed method can locate both single and multiple open-circuit faults. [19], [20] and the proposed method are both low-implemented. In [19], [20], fundamental components are calculated in $\alpha\beta$-axis by calculating the rotating angle, the Fourier series are calculated by FFT in [27], [28], the calculation consume is O($L \log L$). In the proposed method, the fundamental components are approximated by CDR. The calculation complex is O($\log_2 L$). The tuning effort is relatively lower because of the large efficient value ranges of thresholds. Consequently, the proposed method shows advantages in efficiency, calculation consumption, and low implementation.

V. CONCLUSION

Signal spectral analysis based methods are widely used in fault diagnosis. However, the calculation consumes limits the application in the real-time system, such as transistor open-circuit fault diagnosis in VSIs fed IM. In this paper, a real-time, easy-implemented simplified Fourier series algorithm for low-frequency periodic signals by data reconstruction with the position of ZSC is proposed, the Fourier series can be calculated in every sampling instant by product between reconstructed signals and reference signals. Especially, a novel normalized method of DC and fundamental components of simplified Fourier series is proposed to VSIs transistor open-circuit fault location. Comparison results show that the proposed simplified Fourier series algorithm nearly coincides with FFT. Experimental results show the high efficiency of proposed methods, both single and multiple of transistor open-circuit fault can be located in VSIs fed IM.

REFERENCES

[1] S. Yang, A. Bryant, P. Mawby, D. Xiang, L. Ran, and P. Tavner, "An industry-based survey of reliability in power electronic converters," IEEE Trans. Ind. Appl., vol. 47, no. 3, pp. 1441–1451, May 2011.

[2] W. Qiao and D. Lu, "A survey on wind turbine condition monitoring and fault diagnosis-part i: Components and subsystems," IEEE Trans. Ind. Electron., vol. 62, no. 10, pp. 6536–6545, Oct 2015.

[3] M. Riera-Guasp, J. A. Antonino-Daviu, and G. A. Capolino, "Advances in electrical machine, power electronic, and drive condition monitoring and fault detection: State of the art," IEEE Trans. Ind. Electron., vol. 62, no. 3, pp. 1746–1759, March 2015.

[4] S. M. Jung, J. S. Park, H. W. Kim, K. Y. Cho, and M. J. Youn, "An mras-based diagnosis of open-circuit fault in pwm voltage-source inverters for pm synchronous motor drive systems," IEEE Trans. Power Electron., vol. 28, no. 5, pp. 2514–2526, May 2013.

[5] W. Qiao and D. Lu, "A survey on wind turbine condition monitoring and fault diagnosis-part ii: Signals and signal processing methods," IEEE Trans. Ind. Electron., vol. 62, no. 10, pp. 6546–6557, Oct 2015.

[6] I. Jlassi, J. O. Estima, S. K. E. Khil, N. M. Bellaaj, and A. J. M. Cardoso, "Multiple open-circuit faults diagnosis in back-to-back converters of pmsg drives for wind turbine systems," IEEE Trans. Power Electron., vol. 30, no. 5, pp. 2689–2702, May 2015.

[7] B. Lu and S. K. Sharma, "A literature review of igbt fault diagnostic and protection methods for power inverters," IEEE Trans. Ind. Appl., vol. 45, no. 5, pp. 1770–1777, Sept 2009.

[8] M. A. Rodriguez-Blanco, A. Claudio-Sanchez, D. Theilliol, L. G. Vela-Valdes, P. Sibaja-Teran, L. Hernandez-Gonzalez, and J. Aguayo-Alquicira, "A failure-detection strategy for igbt based on gate-voltage behavior applied to a motor drive system," IEEE Trans. Ind. Electron., vol. 58, no. 5, pp. 1625–1633, May 2011.

[9] D. W. Brown, M. Abbas, A. Ginart, I. N. Ali, P. W. Kalgren, and G. J. Vachtsevanos, "Turn-off time as an early indicator of insulated gate bipolar transistor latch-up," IEEE Trans. Power Electron., vol. 27, no. 2, pp. 479–489, Feb 2012.

[10] C. Choi and W. Lee, "Design and evaluation of voltage measurement-based sectoral diagnosis method for inverter open switch faults of permanent magnet synchronous motor drives," IET Electr. Power Appl., vol. 6, no. 8, pp. 526–532, September 2012.

[11] S. Karimi, P. Poure, and S. Saadate, "Fast power switch failure detection for fault tolerant voltage source inverters using fpga," IET Power Electron., vol. 2, no. 4, pp. 346–354, July 2009.

[12] Y. Wang, Z. Li, and L. Lin, "A novel diagnosis method based on flexible error voltage for igbts open-circuit faults in voltage-source inverters," in Industrial Electronics Society, IECON 2015 - 41st Annual Conference of the IEEE, Nov 2015, pp. 000 019–000 024.

[13] C. Shu, C. Ya-ting, Y. Tian-jian, and W. Xun, "A novel diagnostic technique for open-circuited faults of inverters based on output line-to-line voltage model," IEEE Trans. Ind. Electron., vol. PP, no. 99, pp. 1–1, 2016.

[14] N. M. A. Freire, J. O. Estima, and A. J. M. Cardoso, "A voltage-based approach without extra hardware for open-circuit fault diagnosis in closed-loop pwm ac regenerative drives," IEEE Trans. Ind. Electron., vol. 61, no. 9, pp. 4960–4970, Sept 2014.

[15] A. M. S. Mendes, A. J. M. Cardoso, and E. S. Saraiva, "Voltage source inverter fault diagnosis in variable speed ac drives, by park's vector

approach," in Power Electronics and Variable Speed Drives, 1998. Seventh International Conference on (Conf. Publ. No. 456), Sep 1998, pp. 538–543.

[16] A. M. S. Mendes, M. B. Abadi, and S. M. A. Cruz, "Fault diagnostic algorithm for three-level neutral point clamped ac motor drives, based on the average current park's vector," IET Power Electron., vol. 7, no. 5, pp. 1127–1137, May 2014.

[17] F. Zidani, D. Diallo, M. E. H. Benbouzid, and R. Nait-Said, "A fuzzy-based approach for the diagnosis of fault modes in a voltage-fed pwm inverter induction motor drive," IEEE Trans. Ind. Electron., vol. 55, no. 2, pp. 586–593, Feb 2008.

[18] J. Zhang, J. Zhao, D. Zhou, and C. Huang, "High-performance fault diagnosis in pwm voltage-source inverters for vector-controlled induction motor drives," IEEE Trans. Power Electron., vol. 29, no. 11, pp. 6087–6099, Nov 2014.

[19] K. Rothenhagen and F. W. Fuchs, "Performance of diagnosis methods for igbt open circuit faults in three phase voltage source inverters for ac variable speed drives," in Power Electronics and Applications, 2005 European Conference on, Sept 2005, pp. 10 pp.–P.7.

[20] ——, "Performance of diagnosis methods for igbt open circuit faults in voltage source active rectifiers," in Power Electronics Specialists Conference, 2004. PESC 04. 2004 IEEE 35th Annual, vol. 6, June 2004, pp. 4348–4354 Vol.6.

[21] W. Sleszynski, J. Nieznanski, and A. Cichowski, "Open-transistor fault diagnostics in voltage-source inverters by analyzing the load currents," IEEE Trans. Ind. Electron., vol. 56, no. 11, pp. 4681–4688, Nov 2009.

[22] J. O. Estima and A. J. M. Cardoso, "A new algorithm for real-time multiple open-circuit fault diagnosis in voltage-fed pwm motor drives by the reference current errors," IEEE Trans. Ind. Electron., vol. 60, no. 8, pp. 3496–3505, Aug 2013.

[23] F. Wu and J. Zhao, "A real-time multiple open-circuit fault diagnosis method in voltage-source-inverter fed vector controlled drives," IEEE Trans. Power Electron., vol. 31, no. 2, pp. 1425–1437, Feb 2016.

[24] F. Wu, J. Zhao, and Y. Liu, "Symmetry-analysis-based diagnosis method with correlation coefficients for open-circuit fault in inverter," Electron. Lett., vol. 51, no. 21, pp. 1688–1690, 2015.

[25] D.-E. Kim and D.-C. Lee, "Fault diagnosis of three-phase pwm inverters using wavelet and svm," J. Power Electron., vol. 9, no. 3, pp. 377–385, MAY 20 2009.

[26] J. Zhang, H. Luo, J. Zhao, and F. Wu, "A fuzzy-based approach for open-transistor fault diagnosis in voltage-source inverter induction motor drives," Eur. Phys. J. Appl. Phys., vol. 69, p. 20101, 2015.

[27] C. Gan, J. Wu, S. Yang, Y. Hu, W. Cao, and J. Si, "Fault diagnosis scheme for open-circuit faults in switched reluctance motor drives using fast fourier transform algorithm with bus current detection," IET Power Electron., vol. 9, no. 1, pp. 20–30, 2016.

[28] T. Wang, J. Qi, H. Xu, Y. Wang, L. Liu, and D. Gao, "Fault diagnosis method based on fft-rpca-svm for cascaded-multilevel inverter," ISA Trans., vol. 60, pp. 156 – 163, 2016.